https://doi.org/10.5194/egusphere-2023-2684
Preprint. Discussion started: 12 December 2023

Measurement report: Secondary organic aerosols at a forested mountain site in southeastern China

Zijun Zhang[1,2], Weiqi Xu[1,*], Yi Zhang[1,2], Wei Zhou[1], Xiangyu Xu[1,2], Aodong Du[1,2], Yinzhou Zhang[1], Hongqin Qiao[3], Ye Kuang[3], Xiaole Pan[1], Zifa Wang[1,2], Xueling Cheng[1], Lanzhong Liu[4], Qingyan Fu[5], Douglas R. Worsnop[6], Jie Li[1], Yele Sun[1,2,*]

[1]State Key Laboratory of Atmospheric Boundary Layer Physics and Atmospheric Chemistry, Institute of Atmospheric Physics, Chinese Academy of Sciences, Beijing 100029, China
[2]College of Earth and Planetary Sciences, University of Chinese Academy of Sciences, Beijing 100049, China
[3]Institute for Environmental and Climate Research, Jinan University, Guangzhou 511143, China
[4]Shanghuang Atmospheric Boundary Layer and Eco-Environment Observatory, Institute of Atmospheric Physics, Chinese Academy of Sciences, Jinhua 321203, China
[5]Shanghai Environmental Monitoring Center, Shanghai 200235, China
[6]Aerodyne Research Inc., Billerica, Massachusetts 01821, United States

Correspondence to: Weiqi Xu (xuweiqi@mail.iap.ac.cn), Yele Sun (sunyele@mail.iap.ac.cn)

Abstract. Aerosol particles play crucial roles in both climate dynamics and human health. However, there remains a significant gap in our understanding of aerosol composition and evolution, particularly regarding secondary organic aerosols (SOA), and their interaction with clouds in high-altitude background areas in China. Here we conducted real-time measurements of submicron aerosols (PM_1) using aerosol mass spectrometers at a forested mountain site (1128 m a.s.l.) in southeastern China in November 2022. Our results revealed that organic aerosol (OA) constituted a substantial portion of PM_1 (41.1 %), with the OA being primarily of secondary origin, as evidenced by a high oxygen-to-carbon (O/C) ratio (0.85–0.96). Positive matrix factorization resolved two distinct SOA factors: less oxidized oxygenated OA (LO-OOA) and more oxidized OOA (MO-OOA). Interestingly, MO-OOA was scavenged efficiently during cloud events, while cloud evaporation contributed significantly to LO-OOA. The ratio of OA/ΔCO increased with a decrease in the O/C ratio, suggesting that OA remaining in cloud droplets generally maintained a moderate oxidation state. Furthermore, our results indicated a higher contribution of organic nitrates to total nitrate during cloudy periods (27 %) compared to evaporative periods (3 %). Notably, a substantial contribution of nitrate in PM_1 (20.9 %) was observed, particularly during high PM periods, implying that nitrate formed in polluted areas interacted with clouds and significantly impacted the regional background site. Overall, our study underscores the importance of understanding the dynamics of secondary organic aerosols and the impacts of cloud processing in regional mountainous areas in southeastern China.

1 Introduction

Aerosol particles play essential roles in regional and global climate (Ramanathan et al., 2001; Kanakidou et al., 2005), as well as air pollution (Huang et al., 2014) and public health (Kampa and Castanas, 2008). Submicron aerosol (PM_1) from both

https://doi.org/10.5194/egusphere-2023-2684
Preprint. Discussion started: 12 December 2023

natural and anthropogenic sources can be transported to the upper layer of atmospheric boundary layer or even lower free troposphere through convection and frontal uplift (Monks et al., 2009; Huang et al., 2020; Carbone et al., 2014). At high altitudes, aerosol species can be transported over longer distances, depending on their particle sizes and compositions (Pokorná et al., 2022; Tang et al., 2016; Zhong et al., 2022), and the aging processes during transport results in continuous changes in chemical and physical properties (Calvo et al., 2013; Hallquist et al., 2009). High-altitude aerosols can serve as cloud condensation nuclei or ice nuclei, thereby affecting the lifetime and optical properties of clouds (Haywood and Boucher, 2000). They can also have potential impacts on ground-level air pollution through downward mixing (Timonen et al., 2013). As a result, measurements of high-altitude regional aerosols are of great importance for a better understanding of aerosol-cloud interactions and their impacts.

Mountain sites are crucial platforms for studying aerosol characteristics over regional scale and the influences of diverse emission sources (e.g., biomass burning, industrial process, and biogenic emissions) and atmospheric processes (e.g., in-cloud processing, new particle formation). Compared to balloon and aircraft observations, mountain sites have advantages in continuous and long-term observations. In addition, the different meteorological conditions at mountain sites can have great impacts on aerosol formation aerosol formation, aging, and scavenging patterns. For example, Gao et al. (2023) showed that cloud processes can promote the formation of secondary organic aerosol (SOA) by multiphase oxidation. Li et al. (2013) found that high relative humidity (RH) at Mt. Hua can lead to a reduction in particle acidity, and thus reduce the formation of biogenic SOA by suppressing the acid-catalysis reaction. Chen et al. (2021) reported that fog scavenging was more efficient towards particles with aerodynamic diameter larger than 700 nm in Taiwan mountain regions, while smaller particles could continue to grow via gas-to-aqueous partition. Although several studies over mountain sites have been conducted to characterize chemical composition and sources several mountain stations have been settled in China to gain more information on the chemical composition and sources (Zhang et al., 2018; Zhang et al., 2019; Du et al., 2015; Zhang et al., 2014), optical properties (Wang et al., 2015), and hygroscopic properties of aerosols (Ding et al., 2021), most of them are mainly conducted on Qinghai-Tibetan Plateau and in Northern China Plain (NCP), while the studies in southeastern China is very limited.

In this work, a high-resolution time-of-flight aerosol mass spectrometer (AMS hereafter) and a quadruple aerosol chemical speciation monitor (ACSM hereafter) were deployed at a forested mountain site in southeastern China. The chemical composition and properties of PM_1 are characterized, the elemental composition and oxidation state of OA are determined, and the effect of cloud processes on aerosol species is also discussed. The sources of organic aerosol are investigated using positive matrix factorization (PMF) analysis of combined high-resolution organic and inorganic aerosol mass spectra. Particularly, particle organic nitrates (ONs) are determined and quantified based on PMF results. Finally, the potential transport pathways of PM_1 are investigated using backward trajectory analysis.

https://doi.org/10.5194/egusphere-2023-2684
Preprint. Discussion started: 12 December 2023

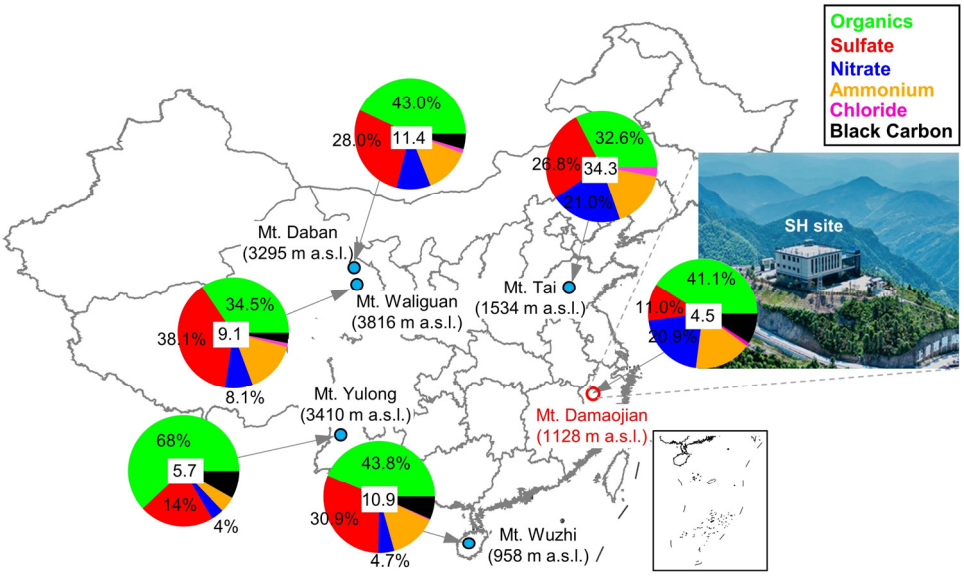

Figure 1. Location of the sampling site. The mean concentration (in μg m-3) and chemical composition of submicron aerosols (NR-PM1+ BC if it was available) measured at selected mountain sites in China are also shown. Detailed information of these sampling sites is presented in Table S1 in the Supplement.

2 Methods

2.1 Site and instrumentation

The campaign was carried out from 1 November to 30 November 2022 at Shanghuang Atmospheric Boundary Layer and Eco-Environment Observatory (SH site) on the top of Mt. Damaojian (119.51°E, 28.58°N, 1128 m a.s.l.) in Wuyi County, Zhejiang Province (Fig. 1). This site is a typical background site in southeastern China that is surrounded by mountains and forests, and there are no strong local anthropogenic sources nearby.

PM_1 species were measured using a suite of real-time instruments with 1−5 min time resolution, including an AMS operated under the "V-mode" and a quadrupole ACSM for non-refractory (NR)-PM_1 composition, together with a seven-wavelength Aethalometer (AE33, Magee Scientific Corp.) for equivalent black carbon (BC) mass concentration. The AMS measurements were only conducted during two periods (15−20 November and 24−28 November, respectively) in this study due to the malfunction of the instrument. Briefly, aerosol particles were sampled into an air-conditioned room through stainless steel tube (O.D.: 1/4 inch), and the residence time was estimated as 5 s. A nafion dryer was placed upstream of the ACSM and AMS to remove the moisture, after that, aerosol particles were sampled into AMS, ACSM, and AE33, respectively. Simultaneously, air pollutants including NO_x, O_3, $PM_{2.5}$, and PM_{10} were measured by gas analyzers (Thermo Scientific Inc., USA), and CO was measured by a Picarro greenhouse gas analyzer (G2401, Picarro Inc., USA). In addition, meteorological parameters containing temperature (*T*), RH, wind speed (WS), wind direction (WD), and pressure (*P*) were measured at the same site.

https://doi.org/10.5194/egusphere-2023-2684
Preprint. Discussion started: 12 December 2023

2.2 Data analysis

2.2.1 ACSM and AMS

ACSM data were analyzed using ACSM standard data analysis software (v2.5.13) and AMS data were analyzed using SQUIRREL v1.65F and PIKA v1.25F. A composition-dependent collection efficiency (CDCE) was applied to the ACSM/AMS data according to Middlebrook et al. (2012). Elemental analysis of high-resolution mass spectra (HRMS) was performed using the "Improved-Ambient" (I-A) method (Canagaratna et al., 2015). The default relative ionization efficiency (RIE) values of 1.1, 1.4, and 1.3 were applied for nitrate, organics, and chloride. According to the ion efficiency (IE) calibration results, the RIE values of ammonium and sulfate were 5.05 and 0.73 for ACSM, and 5.26 and 1.28 for AMS, respectively. As shown in Fig. S1, the concentrations of NR-PM_1 tracked well with $PM_{2.5}$ and PM_{10} measured by gas analyzers (r^2 = 0.70 and 0.66, respectively) suggesting that the AMS/ACSM quantification was reasonable.

PMF Evaluation Tool (PET v3.04) was employed to further deconvolve the HRMS into different source factors following the procedures reported by Ulbrich et al. (2009) and Zhang et al. (2011). In addition to organic fragment ions, the major fragment ions of inorganic species, i.e., SO^+ (*m/z* 48), SO_2^+ (*m/z* 64), SO_3^+ (*m/z* 80), HSO_3^+ (*m/z* 81), $H_2SO_4^+$ (*m/z* 98) for sulfate, NO^+ (*m/z* 30), NO_2^+ (*m/z* 46) for nitrate, NH^+ (*m/z* 15), NH_2^+ (*m/z* 16), NH_3^+ (*m/z* 17) for ammonium, and Cl^+ (*m/z* 35), HCl^+ (*m/z* 36) for chloride were also included into the HR data and error matrices for PMF. A more detailed description of the procedures was given in Sun et al. (2012). After checking the key diagnostic plots (Fig. S2), mass spectra, and the correlations with related tracers, a four-factor solution was considered as the optimal solution in this study.

2.2.2 Estimation of organic nitrates

ONs were estimated from the PMF results (Zhang et al., 2011; Xu et al., 2015). Briefly, NO_x^+ (i.e., NO^+ and NO_2^+) are major fragments of nitrate functionality (-ONO_2), which can be referred to as the total nitrate measured by AMS. Combining inorganic with organic mass spectra in PMF, NO^+ and NO_2^+ can be separated into different organic aerosol (OA) factors and an inorganic nitrate aerosol factor (NIA). Therefore, the mass concentration of ONs ($NO_{3,org}$) was calculated by summing these two ion signals distributed in all OA factors as follows:

$$NO_{3,org} = NO^+_{org} + NO^+_{2,org} \quad (1)$$

$$NO^+_{org} = \sum([\text{OA factor}]_i \times f_{NO^+,i}) \quad (2)$$

$$NO^+_{2,org} = \sum([\text{OA factor}]_i \times f_{NO_2^+,i}) \quad (3)$$

where $[\text{OA factor}]_i$ represents the mass concentration of OA factor *i* resolved by PMF, $f_{NO^+,i}$ and $f_{NO_2^+,i}$ are the mass fractions of NO^+ and NO_2^+ in OA factor *i*, respectively.

https://doi.org/10.5194/egusphere-2023-2684
Preprint. Discussion started: 12 December 2023

2.2.3. Backward trajectory analysis

The Hybrid Single-Particle Lagrangian Integrated Trajectories (HYSPLIT) model and meteorological data from the NOAA Global Data Assimilation System (GDAS) were used to calculate 72 h backward trajectories at the SH site. The trajectory time was set from 0:00 to 23:00 at 1 h intervals, and the height was set as 1100 m. To further show the particle concentration levels in different regions, the map was colored by the time-averaged organic carbon surface mass concentration (ENSEMBLE) from the MERRA-2 model, which was obtained from the NASA Giovanni website (http://giovanni.sci.gsfc.nasa.gov/giovanni).

3. Results and discussion

3.1. General descriptions

Figure 2 shows the time series of meteorological parameters (*T*, RH, WD, and WS), air pollutants ($PM_{2.5}$ and CO) along with PM_1 species during the campaign. The total PM_1 concentration varied dynamically from 0.3 μg m^{-3} to 57.95 μg m^{-3}, with an average (± 1σ) of 4.45 ± 6.51 μg m^{-3}. As shown in Fig. 1, organics held the largest contribution to total PM_1 during the sampling period (41.1 %), followed by nitrate (20.9 %), ammonium (17.0 %), sulfate (11.0 %), BC (9.0 %), and chloride (1.0 %). The concentration and composition of PM_1 are quite different from those observed at other mountain sites with similar altitudes (Fig. 1), such as Mt. Wuzhi, where PM_1 has a mean mass concentration of 10.9 μg m^{-3}, and sulfate makes up a significant part (30.9 %) of total PM_1 (Zhu et al., 2016). Note that the PM_1 concentration at SH site is even lower than those at mountain sites with higher attitude (Fig. 1), such as Mt. Tai (34.3 μg m^{-3}) in NCP (Zhang et al., 2014), Mt. Yulong (5.4 μg m^{-3}) (Zheng et al., 2017), and Mt. Waliguan (9.1 μg m^{-3}) (Zhang et al., 2019). Considering the occurrence of frequent cloud events during the sampling period, the low PM_1 concentration might be mainly associated with cloud scavenging (Kim et al., 2019). Indeed, the unexpectedly high fraction of nitrate at the regional background site might indicate that nitrate formed from anthropogenic-emitted NO_x can have a significant impact on regional scale in the southeastern China. One explanation was that nitrate formed in polluted regions interacted with clouds and affected the regional nitrate level as cloud evaporates (Tao et al., 2018).

Figure 3 shows the relative contribution of each PM_1 component as a function of PM_1 concentration together with the probability density of PM_1 mass loading. The highest two probabilities were distributed within 0–6 μg m^{-3} and 12–18 μg m^{-3} (48.5 % and 30.1 %, respectively). The fraction of nitrate increased significantly with PM_1 concentration, and meanwhile, the fraction of organics and BC exhibited a decreasing trend. This result suggested that high levels of PM_1 at the SH site might be mainly attributed to the nitrate formation and transport. It is also noted that a nitrate-dominant peak of PM_1 mass loading was observed at the nighttime of 4 November (Fig. 2d), which was associated with the corresponding increase in CO, further emphasizing the contribution of transport to nitrate.

https://doi.org/10.5194/egusphere-2023-2684
Preprint. Discussion started: 12 December 2023

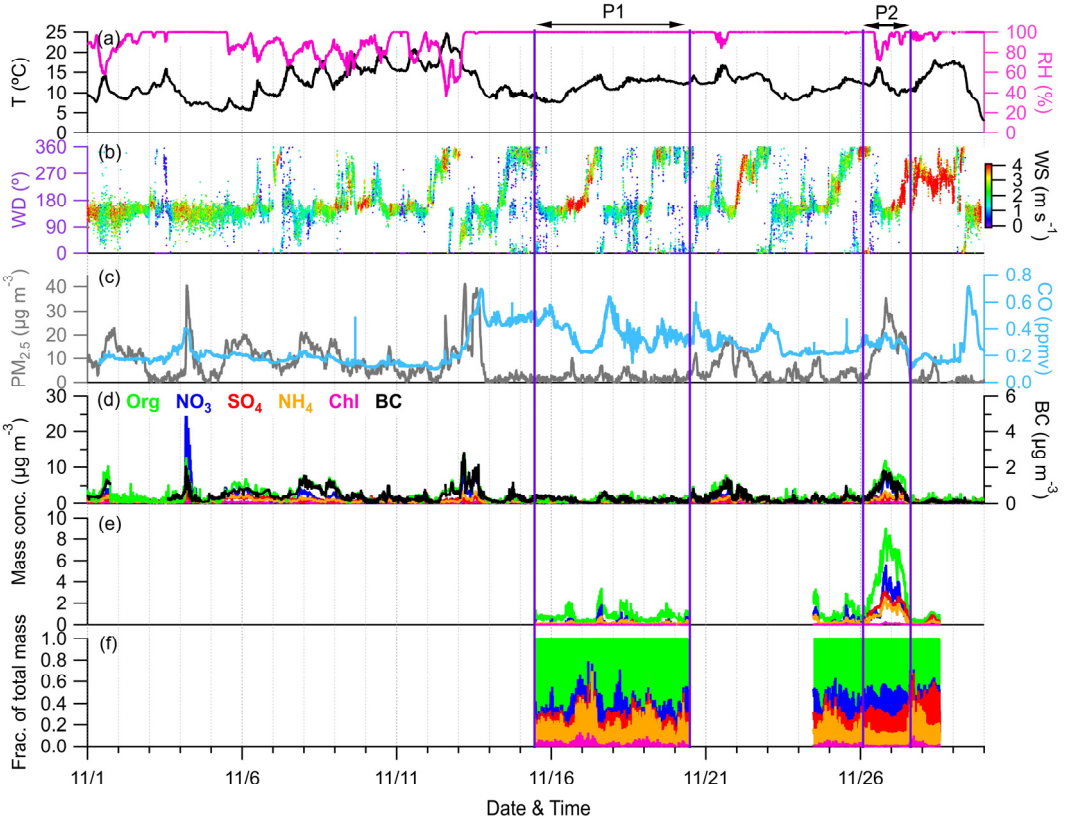

Figure 2. Time series of (a) *T* and RH; (b) WD coloured by WS; (c) mass concentration of $PM_{2.5}$ and mixing ratio of CO; (d) mass concentrations of PM_1 species measured by ACSM; and (e, f) mass concentrations and contributions of PM_1 species measured by AMS.

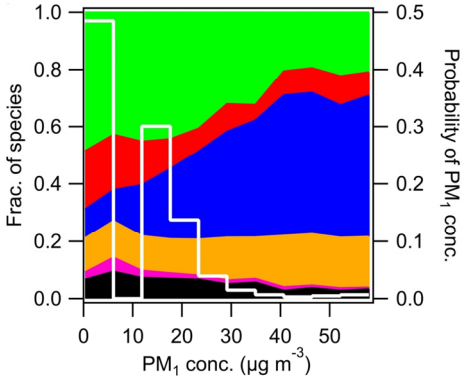

Figure 3. Variations of aerosol composition as a function of PM_1 mass concentration and the probability density of PM_1 during the entire campaign.

https://doi.org/10.5194/egusphere-2023-2684
Preprint. Discussion started: 12 December 2023

The diurnal cycles of PM_1 species, air pollutants, and meteorological parameters during the entire campaign are illustrated in Fig. S3. The mean and median values of organics and nitrate both showed distinct noon peaks at around 14:00, which could be attributed to the daytime photochemical production and the low wind speed (Tang et al., 2022; Xu et al., 2018b). The high nighttime peak of nitrate was mainly due to the influences of the nitrate event on 4 November. Comparatively, sulfate, chloride, and BC showed relatively flat diurnal variations, suggesting the regional characteristics of these species (Zhang et al., 2015).

3.2 Comparisons of two different periods

RH plays a crucial role in determining the composition, formation, and evolution of PM_1 (Sun et al., 2013; Xu et al., 2019). Figure S4 shows the variation of organics, nitrate, and sulfate mass concentrations as a function of RH during the entire campaign. Overall, the mass concentrations of organics decreased significantly with increasing RH, while nitrate and sulfate only showed slight decreases. Previous studies have shown that aerosol mass generally increases on foggy days (Chen et al., 2021). This phenomenon could be due to the cloud scavenging effect under high RH at this site. Another explanation is that submicron aerosols grow to larger sizes under high RH that AMS aerodynamic lens cannot transmit (Chakraborty et al., 2016). To further investigate aerosol characteristics under different meteorological conditions, we selected two periods (Fig. 2, denoted as P1 and P2 hereafter) with largely different humidity and PM_1 concentrations. P1 was a typical cloud scavenging period with relative humidity remaining to be saturated (RH = 100 %), and meanwhile, PM_1 stayed at a very low level, with an average value of 1.34 μg m^{-3}. Whereas in P2, the mean RH decreased to 93.9 % with almost no cloud event, and a high PM_1 event happened with a maximum mass concentration of 20.65 μg m^{-3} (on average 9.39 μg m^{-3}). Then, the PM_1 concentration decreased rapidly due to the enhanced mountain-valley wind (WS > 4 m s^{-1}) and increasing RH (71 % to 100 %) during the nighttime. Therefore, P2 was more likely to be a cloud evaporation period, where aerosol particles were released from the cloud droplets after water evaporation (Fanourgakis et al., 2019).

3.2.1 Size distributions and composition

The average chemically resolved size distributions of NR-PM_1 during P1 and P2 are shown in Fig. 4. Generally, all species were distributed in accumulation mode in both periods. However, a smaller peak size (300–500 nm) and broader size distribution were observed during P1 when compared to those of P2 (~700 nm), probably owing to the wet removal of larger and hygroscopic particles in P1 (Ge et al., 2012). Ammonium showed similar size distribution with sulfate and nitrate during P2, while in P1, it was mixed mainly with sulfate and exhibited a quite different size distribution with nitrate, indicating the potential contribution of organic nitrate.

Clear differences were also found in aerosol composition during P1 and P2. Organics were the dominant contributor to total NR-PM_1 mass during P1 (68 %), followed by nitrate (12 %), ammonium (11 %), and sulfate (8 %). In contrast, despite the decreased contribution of organics (51 %), the mass fractions of sulfate and nitrate increased considerably during P2 (17 % and 19 %, respectively). These changes in the mass fraction of species were attributed to the lower mass scavenging

https://doi.org/10.5194/egusphere-2023-2684
Preprint. Discussion started: 12 December 2023

185 efficiency of organics than inorganic species (Gilardoni et al., 2014). The average HRMS of OA during P1 and P2 are presented in Fig. S5. The HRMS of OA were quite similar for the two periods, with a significant peak *m/z* 44 (mainly CO_2^+). The OA was highly oxidized, with $C_xH_yO_1^+$ dominating the total OA in P1 and P2 by 41 % and 40 %, followed by $C_xH_y^+$ (31 % and 32 %), and $C_xH_yO_2^+$ (20 % and 19 %). The contributions of the two major oxygen-containing ion fragments ($C_xH_yO_1^+$ and $C_xH_yO_2^+$) at the SH site were much higher than those at various urban or suburban sites in China, such as 37.4 % 190 in urban Nanjing (Wang et al., 2016), and 52.9 % in suburban Lanzhou (Tang et al., 2022). Note that higher fraction of CO_2^+ (3 % higher) was found in P1 than P2 (Fig. S5c), indicating a higher oxidation degree of OA in P1 (Xu et al., 2014). This is consistent with the higher O/C and OSc (0.96 and 0.49) in P1 than P2 (0.85 and 0.21).

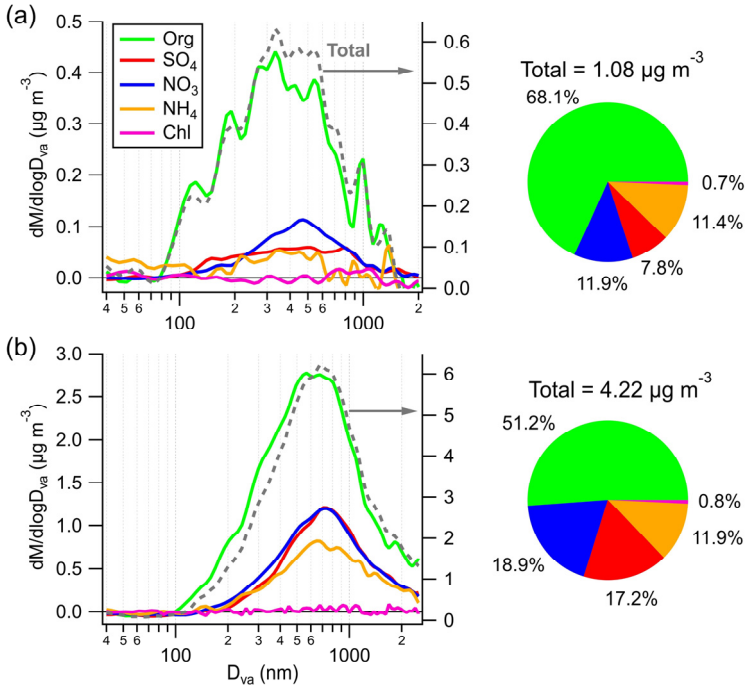

195 **Figure 4.** Averaged size distributions and chemical composition of NR-PM_1 during (a) P1 and (b) P2.

3.2.2 Elemental ratios

Figure 5 shows the time series and box plots of N/C, H/C, OM/OC, O/C, and carbon oxidation state (OSc) of OA, as well as two ion ratios at the SH site. The hourly averaged ratios were only reported for periods with OA concentrations above 0.7 μg 200 m^{-3}. The average N/C ratios were 0.018 for P1 and 0.027 for P2, consistent with the higher fraction of $C_xH_yN_p^+$ in OA during P2. OA had a slightly lower H/C ratio (1.44 vs. 1.48) and higher average ratios of O/C (0.96 vs. 0.85), OM/OC (2.42 vs. 2.29), and OSc (0.49 vs. 0.21) during P1 than those during P2, indicating more oxidized OA during P1. The O/C ratios were

https://doi.org/10.5194/egusphere-2023-2684
Preprint. Discussion started: 12 December 2023

overall within the range of 0.94 ± 0.18 at regional background sites (Zhou et al., 2020), yet much higher than those observed at urban and suburban sites. These results suggest that OA at the SH site was relatively well aged.

The ratio of fragment ions NO^+ (*m/z* 30) to NO_2^+ (*m/z* 46) is a good indicator for identifying the presence of ONs (Farmer et al., 2010; Lin et al., 2021). The mean ratio of NO^+/NO_2^+ in P1 was 4.9, which exceeds the value of 3.88 for pure NH_4NO_3 (AN) obtained from the AMS IE calibration, indicating a potential contribution of ONs. Conversely, the mean NO^+/NO_2^+ in P2 (3.9) was almost identical to that of AN, implying the dominance of inorganic nitrates (INs). Additionally, the $CH_2SO_2^+$ (*m/z* 79) and $CH_3SO_2^+$(*m/z* 80) ions were used as signature fragments of methanesulfonate, a typical organic sulfur species (Chen et al., 2019). However, the mean ratios of $CH_3SO_2^+$ and $CH_2SO_2^+$ during P1 and P2 (0.98 and 1.99, respectively) were lower than the value of 2.9 reported in previous studies for MSA, indicating the negligible contribution of MSA (Song et al., 2019).

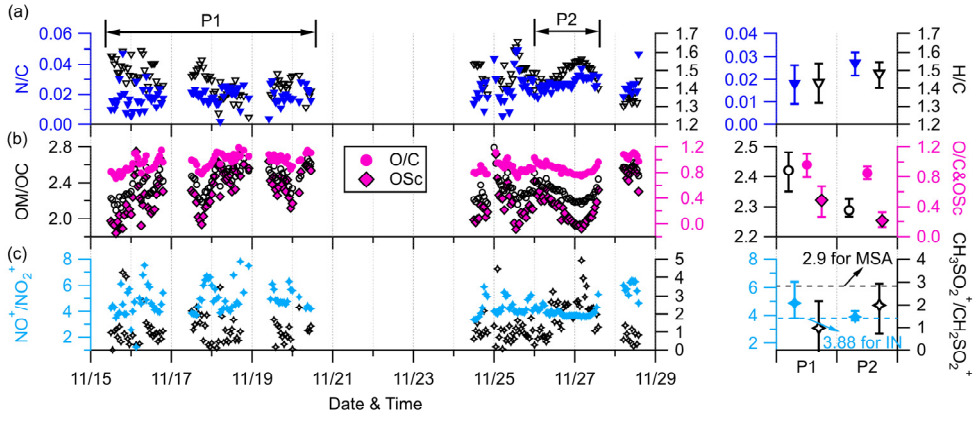

Figure 5. Time series and box plots of 1-hour averaged (a) N/C and H/C, (b) OM/OC, OSc, and O/C, and (c) NO^+/NO_2^+ and $CH_3SO_2^+/CH_2SO_2^+$. Only ratios determined with good S/N (i.e., organics > 0.7 μg m^{-3}) are shown.

3.3 Source apportionment of OA and contribution of organic nitrates

Four factors were resolved by PMF, including three types of SOA and one inorganic factor: less oxidized oxygenated OA (LO-OOA), more oxidized oxygenated OA (MO-OOA), OA associated with sulfate ions (SO_4-OA), and inorganic nitrate aerosol (NIA). These four factors together on average accounted for 87.5 % of the total NR-PM_1 mass. The mass spectra profiles and OA ion family composition of the four factors are shown in Figs. 6 and 7.

https://doi.org/10.5194/egusphere-2023-2684
Preprint. Discussion started: 12 December 2023

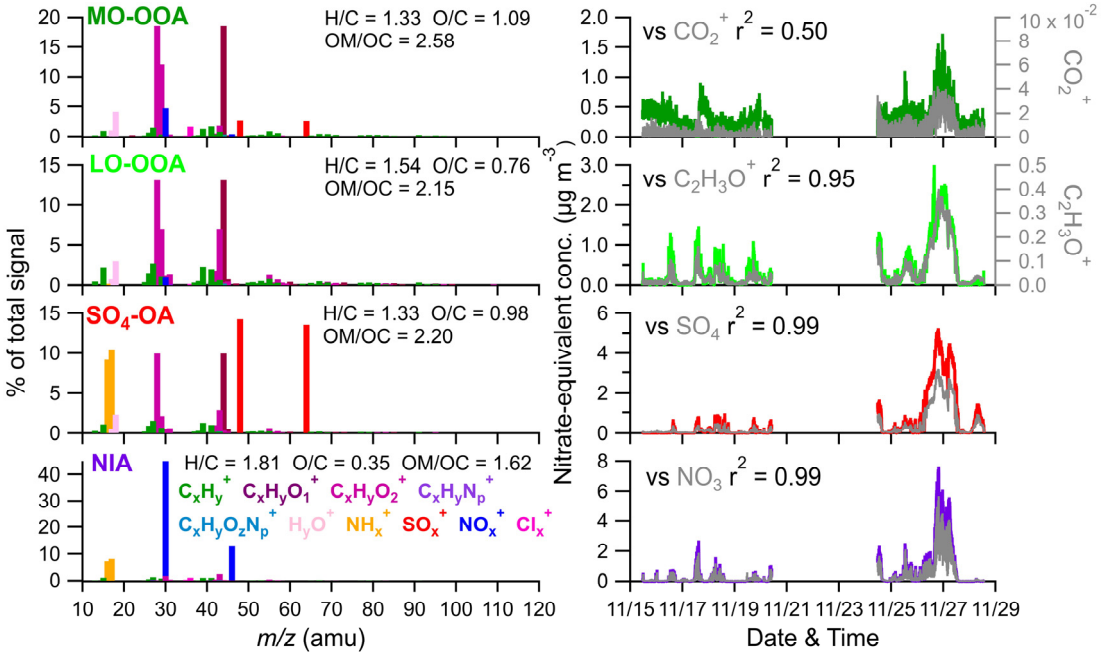

225 **Figure 6.** High-resolution mass spectral profiles (left) and time series (right) of four factors. The correlations of four factors with corresponding tracers are also shown.

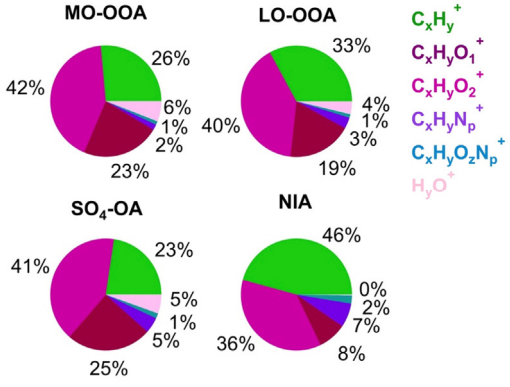

Figure 7. Mass fractional composition of OA ion families for the resolved four PMF factors.

230 LO-OOA and MO-OOA were identified by prominent peaks of CO^+ and CO_2^+ in the mass spectra. LO-OOA had a high fraction of $C_2H_3O^+$ (*m/z* 43, 6.8 % of the total signal), while MO-OOA, corresponding to more oxidized and aged components, had a higher abundance of CO_2^+ (17.6 % vs. 12.8 %), $C_xH_yO_2^+$ (23 % vs. 19 %), and O/C ratio (1.09 vs. 0.76) than LO-OOA. The average O/C ratios of these two OOA factors are similar to those at Mt. Bachelor, where the O/C ratios of SV-OOA and LV-OOA were 0.67 and 1.17, respectively (Zhou et al., 2019). LO-OOA correlated tightly with $C_2H_3O^+$ (r^2 235 = 0.95), and MO-OOA showed a moderate correlation with sulfate (r^2 = 0.56). Overall, the LO-OOA and MO-OOA

https://doi.org/10.5194/egusphere-2023-2684
Preprint. Discussion started: 12 December 2023

components account for 39.1 % and 29.4 % of the total measured OA mass, respectively (Fig. S6). The mass spectra of the SO_4-OA factor had a large amount of NH_x^+ and SO_x^+, together accounting for 48.5 % of the total mass of this factor. Meanwhile, organic components also made up a considerable fraction, yet on average contributing 51 %. It is also noticed that the O/C ratio of the organic fraction of this factor is 0.98, which is even higher than LO-OOA and comparable to MO-OOA, suggesting that this factor has experienced aging processes during the regional transport. Not surprise, no primary OA factor (e.g., hydrocarbon-like OA, biomass burning OA, etc.) was resolved during this study due to the negligible influences of local emissions, which was consistent with the PMF results at other background sites (Zhou et al., 2019; Zhu et al., 2016). A nitrate aerosol factor was also separated from these OA factors, with nitrates in this factor accounting for 92.6 % of the total NO_x^+ ions. Despite NIA, NO_x^+ ions were more assigned in MO-OOA (6.0 % of the total NO_x^+) than LO-OOA (1.4 % of the total NO_x^+), suggesting that ONs were more associated with MO-OOA. According to previous studies, the ratios of NO^+/NO_2^+ for ONs are approximately 2.25–3.7 times higher than pure NH_4NO_3 (Fry et al., 2013; Fry et al., 2009). Consistently, the average NO^+/NO_2^+ ratios of LO-OOA and MO-OOA were 13.19 and 11.2, falling within the range of ONs. In contrast, a NO^+/NO_2^+ ratio of 3.56 was observed for NIA, reflecting its characteristics of inorganic nitrates. Based on the PMF results above, the mass concentrations of ONs during the AMS sampling period were estimated (Fig. 10). Considering ONs as part of organics, we chose a RIE value of 1.4 for the estimated ONs, while a nitrate RIE value (1.1) was correspondingly applied for INs. The results showed that ONs made a greater contribution to total nitrate in P1 than in P2 (27 % vs. 3 %). This was further supported by the result of Huang et al. (2021), which found that organic nitrate can increase rapidly when RH > 70 %. The average mass concentration of ONs in P1 was 30 ng m^{-3}, which was comparable to that in P2 (40 ng m^{-3}), likely owing to the cloud scavenging. Also, the ONs at this site was close to the value (40 ng m^{-3}) obtained at a forest-urban mixed site in Finland (Hao et al., 2014). However, significant discrepancies were observed between the INs mass concentrations during P1 and P2 (0.08 μg m^{-3} vs.1.47 μg m^{-3}), revealing that INs dominated the elevation of total nitrate during cloud evaporation in P2.

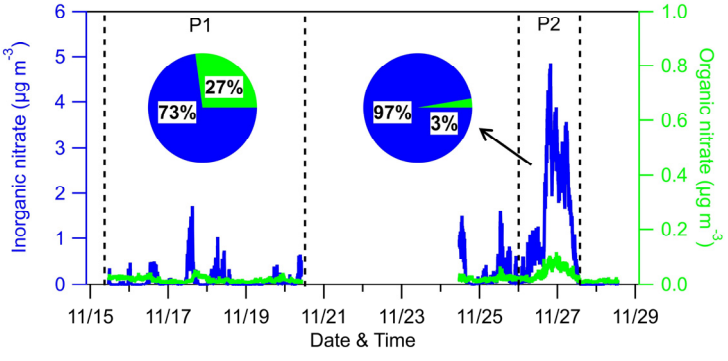

Figure 8. Time series and relative contributions of inorganic nitrate and organic nitrate during the AMS sampling period.

https://doi.org/10.5194/egusphere-2023-2684
Preprint. Discussion started: 12 December 2023

3.4 Evolution of OA

The formation and evolution of OA can be investigated using the ratio of OA to ΔCO (CO minus background CO) to remove the atmospheric dilution effects (Sun et al., 2011). In this study, 0.12 ppmv (average of the lowest 5 % concentration) was used as the background mixing ratio of CO (Fig. S7), which is close to the 0.1 ppm used in Hu et al. (2013) and Yuan et al. (2013). OA/ΔCO was 28.3 ± 26.3 μg m^{-3} $ppmv^{-1}$ during the studing period, which is comparable to (41.7 ± 23.0 μg m^{-3} $ppmv^{-1}$) in suburban Sichuan Basin (Hu et al., 2016) but much lower than the mean value (70 ± 20 μg m^{-3} $ppmv^{-1}$) in worldwide urban air (De Gouw and Jimenez, 2009). The scatter plot of OA/ΔCO as a function of O/C ratios during P1 and P2 is shown in Fig. 9a. Interestingly, different OA/ΔCO variations were found with the increasing O/C during P1 and P2. During P1, OA/ΔCO trended to increase with the increase of the O/C ratio, indicating aging process produced SOA (Hu et al., 2017). In contrast, a remarkable decrease trend of OA/ΔCO was observed with the increasing O/C during P2, suggesting that less oxidized OA may contribute more significantly to the high OA concentration during this period. Moreover, the negative correlation between OA/ΔCO and O/C in P2 also implies that more oxidized OA had almost been scavenged by clouds, while less oxidized OA previously formed or scavenged into cloud droplets was released during cloud evaporation. Similarly, significant increases in the LO-OOA concentration (0.27 to 1.70 μg m^{-3}) and fraction (40 % to 70 %) were observed from P1 to P2, while the MO-OOA concentration (0.40 vs. 0.74 μg m^{-3}) did not show large variation (Fig. 9b), further supporting our conclusion. In addition, these released LO-OOA is likely composed of humic-like substances (HULIS), which can account for 49 % of the water-soluble organic matter at a nearby mountain site in southeastern China (Tao et al., 2023; Chen et al., 2016).

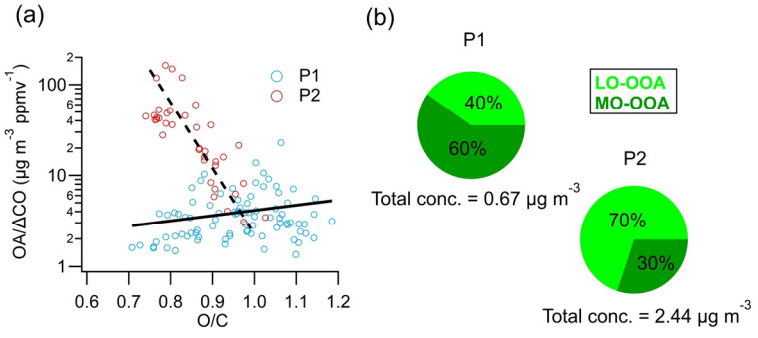

Figure 9. (a) Scatter plot of OA/ΔCO as a function of O/C ratios and (b) mass concentrations and proportions of MO-OOA and LO-OOA during P1 and P2.

Figure 10a shows the Van Krevelen diagrams of OA in this study together with other mountain sites. The slope of H/C to O/C in the present study was -0.66 (r^2 = 0.64), suggesting the addition of carboxyl functional groups during OA evolution (Heald et al., 2010). It is interesting to mention that the two OOA factors exhibited a strong alignment with the fitting line, which suggested that the evolution of OA in this site likely follows a transformation pathway from LO-OOA to MO-OOA.

https://doi.org/10.5194/egusphere-2023-2684
Preprint. Discussion started: 12 December 2023

Consistent evolution trends are also shown in the f_{43} vs. f_{44} space (Fig. 10b). The SO_4-OA and MO-OOA showed similar high oxidative properties, with f_{43} and f_{44} located at the upper part of the triangular region because of the larger fractional contribution of CO_2^+ in the organic mass spectrum. The LO-OOA was situated in the middle region of the triangle, while NIA resided near the bottom right. Moreover, LO-OOA and MO-OOA both overlapped with the aged OAs observed at other elevated sites (Xu et al., 2018a; Zhou et al., 2019). These results together reveal that OA observed at SH site is representative of the background-aged SOA in the YRD region in China.

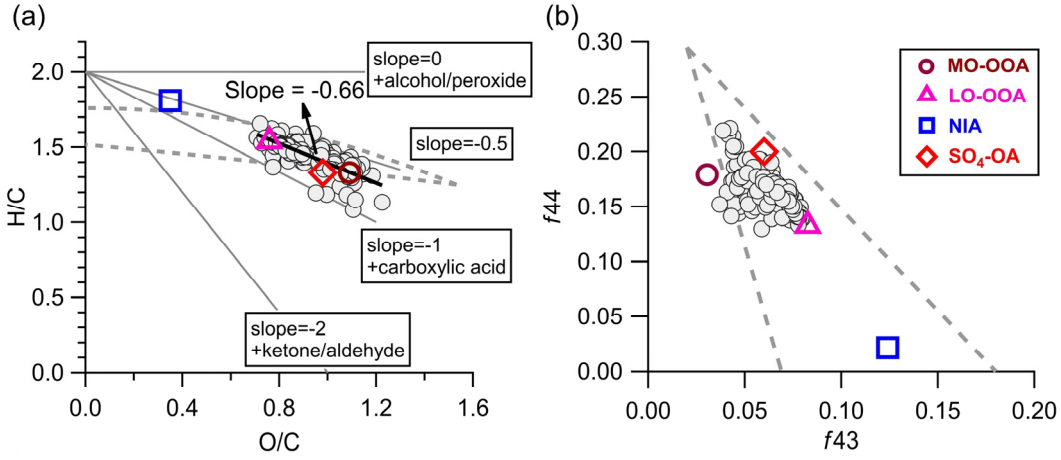

Figure 10. (a) Van Krevelen diagrams (H/C vs. O/C) and (b) f_{43} vs. f_{44} of OA (grey circles, hourly averaged) and four aerosol factors identified by the PMF analyses during the AMS sampling period.

3.5 Backward trajectory analysis

To explore the potential transport pathway of air mass at this background site, 72 h backward trajectories were calculated for the entire campaign (Fig. 11a). Four air mass clusters were determined, including two clusters from the northeast (C1, C3), one from the southwest (C2), and one from the west (C4). Among the four clusters, C2 and C4 exhibited higher air mass contribution (39 % and 35 %) than the other two clusters (18 % and 8 % for C1 and C3, respectively). According to the surface organic carbon data, these two clusters can bring large amounts of aerosols from Jiangxi and Fujian Province to SH site. This influence of C2 and C4 on the particle concentrations at this site is evident in Fig. 11b, where two PM_1 events (Event 2 and 3) were predominantly associated with C2 or C4. These results suggest that the higher levels of PM_1 at the SH site may be heavily influenced by the regional transport of air mass from the west and southwest. Additionally, the nitrate event on 4 November (Event 1, discussed in section 3.1) was primarily linked to C3, indicating a potential long-distance transport contribution of nitrate particles from the NCP region.

https://doi.org/10.5194/egusphere-2023-2684
Preprint. Discussion started: 12 December 2023

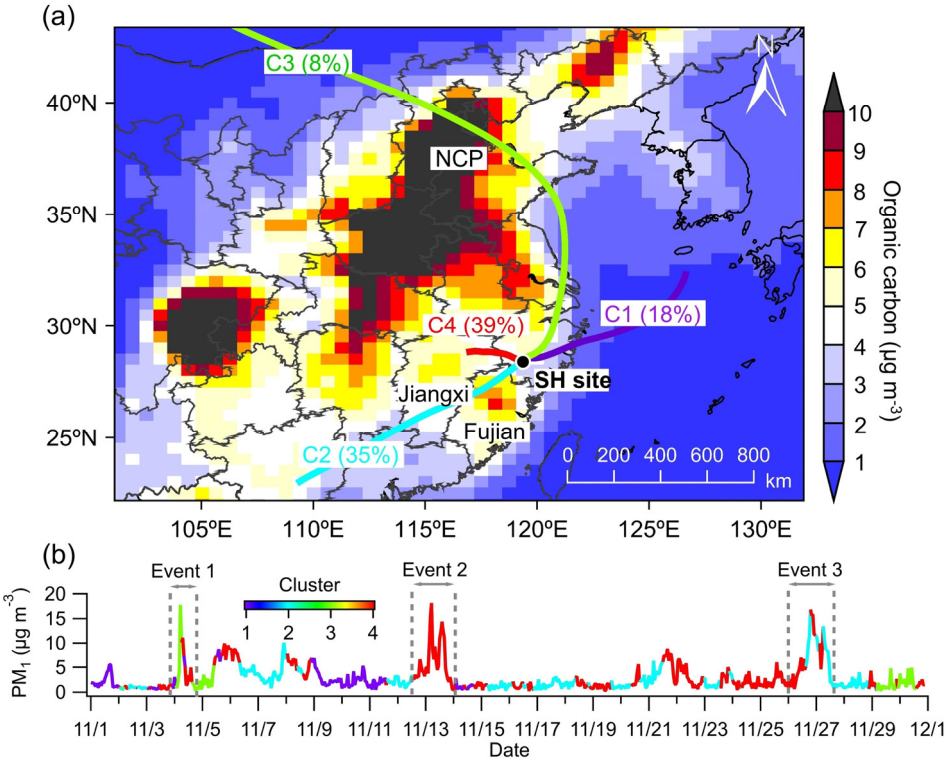

Figure 11. (a) Average 72 h backward trajectory clusters calculated at 1 h intervals during the entire campaign and (b) temporal variation of 1-hour averaged PM_1 concentration coloured by corresponding clusters.

4 Conclusions

The chemical composition and sources of PM_1 were investigated at a forested mountain site in southeastern China in November 2022, by using two different aerosol mass spectrometers. The average mass concentration of total PM_1 (4.45 ± 6.51 μg m^{-3}) was notably lower than those observed at other mountain sites in China, yet similarly dominated by OA (41.1 %). Remarkably, nitrate (20.9 %) and ammonium (17.0 %) exhibited unexpectedly high contributions to PM_1 in this forested mountain area, indicating the impact of anthropogenic emissions on clouds and subsequently influencing regional background areas through atmospheric transport. The OA was primarily of secondary origin and highly aged, as suggested by the high O/C (0.85–0.96) and OSc (0.21–0.49) ratios. PMF analysis of combined organic and inorganic spectra identified two types of SOA. Notably, cloud scavenging and evaporation processes demonstrated differential impacts on LO-OOA and MO-OOA. Cloud scavenging efficiently removed MO-OOA, aligning with smaller size distributions of interstitial particles observed during cloud events. Conversely, cloud evaporation released a substantial amount of LO-OOA, emphasizing that SOA retained in cloud droplets generally maintained a moderate oxidation state. Backward trajectory analysis indicated that higher concentrations of submicron aerosols at the mountain site were associated with transport from the western and southwestern regions. In conclusion, this study underscores the significance of SOA in a forested mountain site in

https://doi.org/10.5194/egusphere-2023-2684
Preprint. Discussion started: 12 December 2023

southeastern China, where aerosol composition, size distributions, and oxidation states are significantly influenced by aerosol-cloud interactions.

Data availability. Data used in this study can be accessed at repository under: https://doi.org/10.5281/zenodo.10312334 (Zhang et al., 2023).

Author contribution. WX and YS designed the research. WX, WZ, and HQ conducted the measurements. ZZ, YZ, WZ, XX, AD, YZ, XC and YS analysed the data. YK, XP, ZW, LL, QF, DRW, and YS reviewed and commented on the paper. ZZ and YS wrote the paper.

Competing interests. The authors declare that they have no conflict of interest.

Acknowledgements. This work was supported by the National Key Research and Development Program of China (No. 2022YFC3703500) and the National Natural Science Foundation of China (No. 42377101).

References

Calvo, A. I., Alves, C., Castro, A., Pont, V., Vicente, A. M., and Fraile, R.: Research on aerosol sources and chemical composition: Past, current and emerging issues, Atmos. Res., 120-121, 1-28, https://doi.org/10.1016/j.atmosres.2012.09.021, 2013.

Canagaratna, M. R., Jimenez, J. L., Kroll, J. H., Chen, Q., Kessler, S. H., Massoli, P., Hildebrandt Ruiz, L., Fortner, E., Williams, L. R., Wilson, K. R., Surratt, J. D., Donahue, N. M., Jayne, J. T., and Worsnop, D. R.: Elemental ratio measurements of organic compounds using aerosol mass spectrometry: characterization, improved calibration, and implications, Atmos. Chem. Phys., 15, 253-272, 10.5194/acp-15-253-2015, 2015.

Carbone, C., Decesari, S., Paglione, M., Giulianelli, L., Rinaldi, M., Marinoni, A., Cristofanelli, P., Didiodato, A., Bonasoni, P., Fuzzi, S., and Facchini, M. C.: 3-year chemical composition of free tropospheric PM1 at the Mt. Cimone GAW global station – South Europe – 2165 m a.s.l, Atmospheric Environment, 87, 218-227, https://doi.org/10.1016/j.atmosenv.2014.01.048, 2014.

Chakraborty, A., Gupta, T., and Tripathi, S. N.: Combined effects of organic aerosol. loading and fog processing on organic aerosols oxidation, composition, and evolution, Sci. Total Environ., 573, 690-698, https://doi.org/10.1016/j.scitotenv.2016.08.156, 2016.

Chen, C.-L., Chen, T.-Y., Hung, H.-M., Tsai, P.-W., Chou, C. C. K., and Chen, W.-N.: The influence of upslope fog on hygroscopicity and chemical composition of aerosols at a forest site in Taiwan, Atmospheric Environment, 246, 118150, https://doi.org/10.1016/j.atmosenv.2020.118150, 2021.

https://doi.org/10.5194/egusphere-2023-2684
Preprint. Discussion started: 12 December 2023

Chen, Q., Ikemori, F., Higo, H., Asakawa, D., and Mochida, M.: Chemical Structural. Characteristics of HULIS and Other Fractionated Organic Matter in Urban Aerosols: Results from Mass Spectral and FT-IR Analysis, Environmental Science & Technology, 50, 1721-1730, 10.1021/acs.est.5b05277, 2016.

Chen, Y., Xu, L., Humphry, T., Hettiyadura, A. P. S., Ovadnevaite, J., Huang, S., Poulain, L., Schroder, J. C., Campuzano-Jost, P., Jimenez, J. L., Herrmann, H., O'Dowd, C., Stone, E. A., and Ng, N. L.: Response of the Aerodyne Aerosol Mass Spectrometer to Inorganic Sulfates and Organosulfur Compounds: Applications in Field and Laboratory Measurements, Environ. Sci. Technol., 53, 5176-5186, 10.1021/acs.est.9b00884, 2019.

De Gouw, J. and Jimenez, J. L.: Organic Aerosols in the Earth's Atmosphere, Environ. Sci. Technol., 43, 7614-7618, 10.1021/es9006004, 2009.

Ding, S., Liu, D., Hu, K., Zhao, D., Tian, P., Wang, F., Li, R., Chen, Y., He, H., Huang, M., and Ding, D.: Optical and hygroscopic properties of black carbon influenced by particle microphysics at the top of the anthropogenically polluted boundary layer, Atmos. Chem. Phys., 21, 681-694, 10.5194/acp-21-681-2021, 2021.

Du, W., Sun, Y. L., Xu, Y. S., Jiang, Q., Wang, Q. Q., Yang, W., Wang, F., Bai, Z. P., Zhao, X. D., and Yang, Y. C.: Chemical characterization of submicron aerosol and particle growth events at a national background site (3295 m a.s.l.) on the Tibetan Plateau, Atmos. Chem. Phys., 15, 10811-10824, 10.5194/acp-15-10811-2015, 2015.

Fanourgakis, G. S., Kanakidou, M., Nenes, A., Bauer, S. E., Bergman, T., Carslaw, K. S., Grini, A., Hamilton, D. S., Johnson, J. S., Karydis, V. A., Kirkevåg, A., Kodros, J. K., Lohmann, U., Luo, G., Makkonen, R., Matsui, H., Neubauer, D., Pierce, J. R., Schmale, J., Stier, P., Tsigaridis, K., van Noije, T., Wang, H., Watson-Parris, D., Westervelt, D. M., Yang, Y., Yoshioka, M., Daskalakis, N., Decesari, S., Gysel-Beer, M., Kalivitis, N., Liu, X., Mahowald, N. M., Myriokefalitakis, S., Schrödner, R., Sfakianaki, M., Tsimpidi, A. P., Wu, M., and Yu, F.: Evaluation of global simulations of aerosol particle and cloud condensation nuclei number, with implications for cloud droplet formation, Atmos. Chem. Phys., 19, 8591-8617, 10.5194/acp-19-8591-2019, 2019.

Farmer, D. K., Matsunaga, A., Docherty, K. S., Surratt, J. D., Seinfeld, J. H., Ziemann, P. J., and Jimenez, J. L.: Response of an aerosol mass spectrometer to organonitrates and organosulfates and implications for atmospheric chemistry, Proceedings of the National Academy of Sciences, 107, 6670-6675, doi:10.1073/pnas.0912340107, 2010.

Fry, J. L., Kiendler-Scharr, A., Rollins, A. W., Wooldridge, P. J., Brown, S. S., Fuchs, H., Dubé, W., Mensah, A., dal Maso, M., Tillmann, R., Dorn, H. P., Brauers, T., and Cohen, R. C.: Organic nitrate and secondary organic aerosol yield from NO₃ oxidation of β-pinene evaluated using a gas-phase kinetics/aerosol partitioning model, Atmos. Chem. Phys., 9, 1431-1449, 10.5194/acp-9-1431-2009, 2009.

Fry, J. L., Draper, D. C., Zarzana, K. J., Campuzano-Jost, P., Day, D. A., Jimenez, J. L., Brown, S. S., Cohen, R. C., Kaser, L., Hansel, A., Cappellin, L., Karl, T., Hodzic Roux, A., Turnipseed, A., Cantrell, C., Lefer, B. L., and Grossberg, N.: Observations of gas- and aerosol-phase organic nitrates at BEACHON-RoMBAS 2011, Atmos. Chem. Phys., 13, 8585-8605, 10.5194/acp-13-8585-2013, 2013.

https://doi.org/10.5194/egusphere-2023-2684
Preprint. Discussion started: 12 December 2023

Gao, M., Zhou, S., He, Y., Zhang, G., Ma, N., Li, Y., Li, F., Yang, Y., Peng, L., Zhao, J., Bi, X., Hu, W., Sun, Y., Wang, B., and Wang, X.: In Situ Observation of Multiphase Oxidation-Driven Secondary Organic Aerosol Formation during Cloud Processing at a Mountain Site in Southern China, Environ. Sci. Technol. Lett., 10, 573-581, 10.1021/acs.estlett.3c00331, 2023.

Ge, X., Zhang, Q., Sun, Y., Ruehl, C. R., and Setyan, A.: Effect of aqueous-phase. processing on aerosol chemistry and size distributions in Fresno, California, during wintertime, Environmental Chemistry, 9, 221-235, 2012.

Gilardoni, S., Massoli, P., Giulianelli, L., Rinaldi, M., Paglione, M., Pollini, F., Lanconelli, C., Poluzzi, V., Carbone, S., Hillamo, R., Russell, L. M., Facchini, M. C., and Fuzzi, S.: Fog scavenging of organic and inorganic aerosol in the Po Valley, Atmos. Chem. Phys., 14, 6967-6981, 10.5194/acp-14-6967-2014, 2014.

Hallquist, M., Wenger, J. C., Baltensperger, U., Rudich, Y., Simpson, D., Claeys, M., Dommen, J., Donahue, N. M., George, C., Goldstein, A. H., Hamilton, J. F., Herrmann, H., Hoffmann, T., Iinuma, Y., Jang, M., Jenkin, M. E., Jimenez, J. L., Kiendler-Scharr, A., Maenhaut, W., McFiggans, G., Mentel, T. F., Monod, A., Prevot, A. S. H., Seinfeld, J. H., Surratt, J. D., Szmigielski, R., and Wildt, J.: The formation, properties and impact of secondary organic aerosol: current and emerging issues, Atmos. Chem. Phys., 9, 5155-5236, 10.5194/acp-9-5155-2009, 2009.

Hao, L. Q., Kortelainen, A., Romakkaniemi, S., Portin, H., Jaatinen, A., Leskinen, A., Komppula, M., Miettinen, P., Sueper, D., Pajunoja, A., Smith, J. N., Lehtinen, K. E. J., Worsnop, D. R., Laaksonen, A., and Virtanen, A.: Atmospheric submicron aerosol composition and particulate organic nitrate formation in a boreal forestland–urban mixed region, Atmos. Chem. Phys., 14, 13483-13495, 10.5194/acp-14-13483-2014, 2014.

Haywood, J. and Boucher, O.: Estimates of the direct and indirect radiative forcing. due to tropospheric aerosols: A review, Reviews of Geophysics, 38, 513-543, 10.1029/1999rg000078, 2000.

Heald, C. L., Kroll, J. H., Jimenez, J. L., Docherty, K. S., DeCarlo, P. F., Aiken, A. C., Chen, Q., Martin, S. T., Farmer, D. K., and Artaxo, P.: A simplified description of the evolution of organic aerosol composition in the atmosphere, Geophys. Res. Lett., 37, https://doi.org/10.1029/2010GL042737, 2010.

Hu, W., Hu, M., Hu, W. W., Zheng, J., Chen, C., Wu, Y., and Guo, S.: Seasonal. variations in high time-resolved chemical compositions, sources, and evolution of atmospheric submicron aerosols in the megacity Beijing, Atmos. Chem. Phys., 17, 9979-10000, 10.5194/acp-17-9979-2017, 2017.

Hu, W., Hu, M., Hu, W. W., Niu, H., Zheng, J., Wu, Y., Chen, W., Chen, C., Li, L., Shao, M., Xie, S., and Zhang, Y.: Characterization of submicron aerosols influenced by biomass burning at a site in the Sichuan Basin, southwestern China, Atmos. Chem. Phys., 16, 13213-13230, 10.5194/acp-16-13213-2016, 2016.

Hu, W. W., Hu, M., Yuan, B., Jimenez, J. L., Tang, Q., Peng, J. F., Hu, W., Shao, M., Wang, M., Zeng, L. M., Wu, Y. S., Gong, Z. H., Huang, X. F., and He, L. Y.: Insights on organic aerosol aging and the influence of coal combustion at a regional receptor site of central eastern China, Atmos. Chem. Phys., 13, 10095-10112, 10.5194/acp-13-10095-2013, 2013.

Huang, R. J., Zhang, Y. L., Bozzetti, C., Ho, K. F., Cao, J. J., Han, Y. M., Daellenbach, K. R., Slowik, J. G., Platt, S. M., Canonaco, F., Zotter, P., Wolf, R., Pieber, S. M., Bruns, E. A., Crippa, M., Ciarelli, G., Piazzalunga, A., Schwikowski, M.,

https://doi.org/10.5194/egusphere-2023-2684
Preprint. Discussion started: 12 December 2023

Abbaszade, G., Schnelle-Kreis, J., Zimmermann, R., An, Z. S., Szidat, S., Baltensperger, U., El Haddad, I., and Prevot, A. S. H.: High secondary aerosol contribution to particulate pollution during haze events in China, Nature, 514, 218-222, 10.1038/nature13774, 2014.

Huang, W., Yang, Y., Wang, Y., Gao, W., Li, H., Zhang, Y., Li, J., Zhao, S., Yan, Y., Ji, D., Tang, G., Liu, Z., Wang, L., Zhang, R., and Wang, Y.: Exploring the inorganic and organic nitrate aerosol formation regimes at a suburban site on the North China Plain, Sci. Total Environ., 768, 144538, https://doi.org/10.1016/j.scitotenv.2020.144538, 2021.

Huang, X., Ding, A. J., Wang, Z. L., Ding, K., Gao, J., Chai, F. H., and Fu, C. B.: Amplified transboundary transport of haze by aerosol-boundary layer interaction in China, Nat. Geosci., 13, 428-+, 10.1038/s41561-020-0583-4, 2020.

Kampa, M. and Castanas, E.: Human health effects of air pollution, Environmental. Pollution, 151, 362-367, https://doi.org/10.1016/j.envpol.2007.06.012, 2008.

Kanakidou, M., Seinfeld, J. H., Pandis, S. N., Barnes, I., Dentener, F. J., Facchini, M. C., Van Dingenen, R., Ervens, B., Nenes, A., Nielsen, C. J., Swietlicki, E., Putaud, J. P., Balkanski, Y., Fuzzi, S., Horth, J., Moortgat, G. K., Winterhalter, R., Myhre, C. E. L., Tsigaridis, K., Vignati, E., Stephanou, E. G., and Wilson, J.: Organic aerosol and global climate modelling: a review, Atmos. Chem. Phys., 5, 1053-1123, 10.5194/acp-5-1053-2005, 2005.

Kim, H., Collier, S., Ge, X., Xu, J., Sun, Y., Jiang, W., Wang, Y., Herckes, P., and. Zhang, Q.: Chemical processing of water-soluble species and formation of secondary organic aerosol in fogs, Atmospheric Environment, 200, 158-166, https://doi.org/10.1016/j.atmosenv.2018.11.062, 2019.

Li, J. J., Wang, G. H., Cao, J. J., Wang, X. M., and Zhang, R. J.: Observation of. biogenic secondary organic aerosols in the atmosphere of a mountain site in central China: temperature and relative humidity effects, Atmos. Chem. Phys., 13, 11535-11549, 10.5194/acp-13-11535-2013, 2013.

Lin, C., Huang, R.-J., Duan, J., Zhong, H., and Xu, W.: Primary and Secondary Organic Nitrate in Northwest China: A Case Study, Environ. Sci. Technol. Lett., 8, 947-953, 10.1021/acs.estlett.1c00692, 2021.

Middlebrook, A. M., Bahreini, R., Jimenez, J. L., and Canagaratna, M. R.: Evaluation of Composition-Dependent Collection Efficiencies for the Aerodyne Aerosol Mass Spectrometer using Field Data, Aerosol Science and Technology, 46, 258-271, 10.1080/02786826.2011.620041, 2012.

Monks, P. S., Granier, C., Fuzzi, S., Stohl, A., Williams, M. L., Akimoto, H., Amann, M., Baklanov, A., Baltensperger, U., Bey, I., Blake, N., Blake, R. S., Carslaw, K., Cooper, O. R., Dentener, F., Fowler, D., Fragkou, E., Frost, G. J., Generoso, S., Ginoux, P., Grewe, V., Guenther, A., Hansson, H. C., Henne, S., Hjorth, J., Hofzumahaus, A., Huntrieser, H., Isaksen, I. S. A., Jenkin, M. E., Kaiser, J., Kanakidou, M., Klimont, Z., Kulmala, M., Laj, P., Lawrence, M. G., Lee, J. D., Liousse, C., Maione, M., McFiggans, G., Metzger, A., Mieville, A., Moussiopoulos, N., Orlando, J. J., O'Dowd, C. D., Palmer, P. I., Parrish, D. D., Petzold, A., Platt, U., Pöschl, U., Prévôt, A. S. H., Reeves, C. E., Reimann, S., Rudich, Y., Sellegri, K., Steinbrecher, R., Simpson, D., ten Brink, H., Theloke, J., van der Werf, G. R., Vautard, R., Vestreng, V., Vlachokostas, C., and von Glasow, R.: Atmospheric composition change – global and regional air quality, Atmospheric Environment, 43, 5268-5350, https://doi.org/10.1016/j.atmosenv.2009.08.021, 2009.

https://doi.org/10.5194/egusphere-2023-2684
Preprint. Discussion started: 12 December 2023

Pokorná, P., Zíková, N., Vodička, P., Lhotka, R., Mbengue, S., Holubová Šmejkalová, A., Riffault, V., Ondráček, J., Schwarz, J., and Ždímal, V.: Chemically speciated mass size distribution, particle density, shape and origin of non-refractory PM1 measured at a rural background site in central Europe, Atmos. Chem. Phys., 22, 5829-5858, 10.5194/acp-22-5829-2022, 2022.

Ramanathan, V., Crutzen, P. J., Kiehl, J. T., and Rosenfeld, D.: Atmosphere - Aerosols, climate, and the hydrological cycle, Science, 294, 2119-2124, 10.1126/science.1064034, 2001.

Song, S., Gao, M., Xu, W., Sun, Y., Worsnop, D. R., Jayne, J. T., Zhang, Y., Zhu, L., Li, M., Zhou, Z., Cheng, C., Lv, Y., Wang, Y., Peng, W., Xu, X., Lin, N., Wang, Y., Wang, S., Munger, J. W., Jacob, D. J., and McElroy, M. B.: Possible heterogeneous chemistry of hydroxymethanesulfonate (HMS) in northern China winter haze, Atmos. Chem. Phys., 19, 1357-1371, 10.5194/acp-19-1357-2019, 2019.

Sun, Y., Wang, Z., Fu, P., Jiang, Q., Yang, T., Li, J., and Ge, X.: The impact of relative humidity on aerosol composition and evolution processes during wintertime in Beijing, China, Atmospheric Environment, 77, 927-934, https://doi.org/10.1016/j.atmosenv.2013.06.019, 2013.

Sun, Y. L., Zhang, Q., Schwab, J. J., Yang, T., Ng, N. L., and Demerjian, K. L.: Factor analysis of combined organic and inorganic aerosol mass spectra from high resolution aerosol mass spectrometer measurements, Atmos. Chem. Phys., 12, 8537-8551, 10.5194/acp-12-8537-2012, 2012.

Sun, Y. L., Zhang, Q., Schwab, J. J., Chen, W. N., Bae, M. S., Lin, Y. C., Hung, H. M., and Demerjian, K. L.: A case study of aerosol processing and evolution in summer in New York City, Atmos. Chem. Phys., 11, 12737-12750, 10.5194/acp-11-12737-2011, 2011.

Tang, C., Zhang, X., Tian, P., Guan, X., Lin, Y., Pang, S., Guo, Q., Du, T., Zhang, Z., Zhang, M., Xu, J., and Zhang, L.: Chemical characteristics and regional transport of submicron particulate matter at a suburban site near Lanzhou, China, Environ. Res., 212, 113179, https://doi.org/10.1016/j.envres.2022.113179, 2022.

Tang, L., Yu, H., Ding, A., Zhang, Y., Qin, W., Wang, Z., Chen, W., Hua, Y., and Yang, X.: Regional contribution to PM1 pollution during winter haze in Yangtze River Delta, China, Sci. Total Environ., 541, 161-166, https://doi.org/10.1016/j.scitotenv.2015.05.058, 2016.

Tao, J., Zhang, Z., Tan, H., Zhang, L., Wu, Y., Sun, J., Che, H., Cao, J., Cheng, P., Chen, L., and Zhang, R.: Observational evidence of cloud processes contributing to daytime elevated nitrate in an urban atmosphere, Atmospheric Environment, 186, 209-215, https://doi.org/10.1016/j.atmosenv.2018.05.040, 2018.

Tao, J., Zhang, Z., Zhang, L., Wu, Y., Ren, Y., Li, J., Huang, J., Wang, G., Shen, Z., Zhang, R., and Wang, B.: Characterization and sources of water-soluble organic species in PM2.5 in a remote mountain environment in Southeastern China, Atmospheric Environment, 313, 120057, https://doi.org/10.1016/j.atmosenv.2023.120057, 2023.

Timonen, H., Wigder, N., and Jaffe, D.: Influence of background particulate matter. (PM) on urban air quality in the Pacific Northwest, Journal of Environmental Management, 129, 333-340, https://doi.org/10.1016/j.jenvman.2013.07.023, 2013.

https://doi.org/10.5194/egusphere-2023-2684
Preprint. Discussion started: 12 December 2023

Ulbrich, I. M., Canagaratna, M. R., Zhang, Q., Worsnop, D. R., and Jimenez, J. L.: Interpretation of organic components from Positive Matrix Factorization of aerosol mass spectrometric data, Atmos. Chem. Phys., 9, 2891-2918, 10.5194/acp-9-2891-2009, 2009.

Wang, J., Ge, X., Chen, Y., Shen, Y., Zhang, Q., Sun, Y., Xu, J., Ge, S., Yu, H., and Chen, M.: Highly time-resolved urban aerosol characteristics during springtime in Yangtze River Delta, China: insights from soot particle aerosol mass spectrometry, Atmos. Chem. Phys., 16, 9109-9127, 10.5194/acp-16-9109-2016, 2016.

Wang, Q. Y., Huang, R. J., Cao, J. J., Tie, X. X., Ni, H. Y., Zhou, Y. Q., Han, Y. M., Hu, T. F., Zhu, C. S., Feng, T., Li, N., and Li, J. D.: Black carbon aerosol in winter northeastern Qinghai–Tibetan Plateau, China: the source, mixing state and optical property, Atmos. Chem. Phys., 15, 13059-13069, 10.5194/acp-15-13059-2015, 2015.

Xu, J., Zhang, Q., Chen, M., Ge, X., Ren, J., and Qin, D.: Chemical composition, sources, and processes of urban aerosols during summertime in northwest China: insights from high-resolution aerosol mass spectrometry, Atmos. Chem. Phys., 14, 12593-12611, 10.5194/acp-14-12593-2014, 2014.

Xu, J., Zhang, Q., Shi, J., Ge, X., Xie, C., Wang, J., Kang, S., Zhang, R., and Wang, Y.: Chemical characteristics of submicron particles at the central Tibetan Plateau: insights from aerosol mass spectrometry, Atmos. Chem. Phys., 18, 427-443, 10.5194/acp-18-427-2018, 2018a.

Xu, J., Zhu, F., Wang, S., Zhao, X., Zhang, M., Ge, X., Wang, J., Tian, W., Wang, L., Yang, L., Ding, L., Lu, X., Chen, X., Zheng, Y., and Guo, Z.: Impacts of relative humidity on fine aerosol properties via environmental wind tunnel experiments, Atmospheric Environment, 206, 21-29, https://doi.org/10.1016/j.atmosenv.2019.03.002, 2019.

Xu, L., Suresh, S., Guo, H., Weber, R. J., and Ng, N. L.: Aerosol characterization over. the southeastern United States using high-resolution aerosol mass spectrometry: spatial and seasonal variation of aerosol composition and sources with a focus on organic nitrates, Atmos. Chem. Phys., 15, 7307-7336, 10.5194/acp-15-7307-2015, 2015.

Xu, P., Zhang, J., Ji, D., Liu, Z., Tang, G., Jiang, C., and Wang, Y.: Characterization of submicron particles during autumn in Beijing, China, Journal of Environmental Sciences, 63, 16-27, https://doi.org/10.1016/j.jes.2017.03.036, 2018b.

Yuan, B., Hu, W. W., Shao, M., Wang, M., Chen, W. T., Lu, S. H., Zeng, L. M., and. Hu, M.: VOC emissions, evolutions and contributions to SOA formation at a receptor site in eastern China, Atmos. Chem. Phys., 13, 8815-8832, 10.5194/acp-13-8815-2013, 2013.

Zhang, Q., Jimenez, J. L., Canagaratna, M. R., Ulbrich, I. M., Ng, N. L., Worsnop, D. R., and Sun, Y.: Understanding atmospheric organic aerosols via factor analysis of aerosol mass spectrometry: a review, Analytical and Bioanalytical Chemistry, 401, 3045-3067, 10.1007/s00216-011-5355-y, 2011.

Zhang, X., Xu, J., Kang, S., Liu, Y., and Zhang, Q.: Chemical characterization of long-range transport biomass burning emissions to the Himalayas: insights from high-resolution aerosol mass spectrometry, Atmos. Chem. Phys., 18, 4617-4638, 10.5194/acp-18-4617-2018, 2018.

https://doi.org/10.5194/egusphere-2023-2684
Preprint. Discussion started: 12 December 2023

Zhang, X., Xu, J., Kang, S., Zhang, Q., and Sun, J.: Chemical characterization and. sources of submicron aerosols in the northeastern Qinghai–Tibet Plateau: insights from high-resolution mass spectrometry, Atmos. Chem. Phys., 19, 7897-7911, 10.5194/acp-19-7897-2019, 2019.

Zhang, Y. J., Tang, L. L., Wang, Z., Yu, H. X., Sun, Y. L., Liu, D., Qin, W., Canonaco, F., Prévôt, A. S. H., Zhang, H. L., and Zhou, H. C.: Insights into characteristics, sources, and evolution of submicron aerosols during harvest seasons in the Yangtze River delta region, China, Atmos. Chem. Phys., 15, 1331-1349, 10.5194/acp-15-1331-2015, 2015.

Zhang, Y. M., Zhang, X. Y., Sun, J. Y., Hu, G. Y., Shen, X. J., Wang, Y. Q., Wang, T. T., Wang, D. Z., and Zhao, Y.: Chemical composition and mass size distribution of PM₁ at an elevated site in central east China, Atmos. Chem. Phys., 14, 12237-12249, 10.5194/acp-14-12237-2014, 2014.

Zheng, J., Hu, M., Du, Z., Shang, D., Gong, Z., Qin, Y., Fang, J., Gu, F., Li, M., Peng, J., Li, J., Zhang, Y., Huang, X., He, L., Wu, Y., and Guo, S.: Influence of biomass burning from South Asia at a high-altitude mountain receptor site in China, Atmos. Chem. Phys., 17, 6853-6864, 10.5194/acp-17-6853-2017, 2017.

Zhong, H., Huang, R. J., Lin, C., Xu, W., Duan, J., Gu, Y., Huang, W., Ni, H., Zhu, C., You, Y., Wu, Y., Zhang, R., Ovadnevaite, J., Ceburnis, D., and O'Dowd, C. D.: Measurement report: On the contribution of long-distance transport to the secondary aerosol formation and aging, Atmos. Chem. Phys., 22, 9513-9524, 10.5194/acp-22-9513-2022, 2022.

Zhou, S., Collier, S., Jaffe, D. A., and Zhang, Q.: Free tropospheric aerosols at the Mt. Bachelor Observatory: more oxidized and higher sulfate content compared to boundary layer aerosols, Atmos. Chem. Phys., 19, 1571-1585, 10.5194/acp-19-1571-2019, 2019.

Zhou, W., Xu, W., Kim, H., Zhang, Q., Fu, P., Worsnop, D. R., and Sun, Y.: A review. of aerosol chemistry in Asia: insights from aerosol mass spectrometer measurements, Environmental Science: Processes & Impacts, 22, 1616-1653, 10.1039/D0EM00212G, 2020.

Zhu, Q., He, L. Y., Huang, X. F., Cao, L. M., Gong, Z. H., Wang, C., Zhuang, X., and Hu, M.: Atmospheric aerosol compositions and sources at two national background sites in northern and southern China, Atmos. Chem. Phys., 16, 10283-10297, 10.5194/acp-16-10283-2016, 2016.